# Spin-Isomer Conversion of Water at Room Temperature and Quantum-Rotor-Induced Nuclear Polarization in the Water-Endofullerene $H_2O@C_{60}$

Benno Meier,[*] Karel Kouřil, Christian Bengs, Hana Kouřilová, Timothy C. Barker, Stuart J. Elliott,
Shamim Alom, Richard J. Whitby, and Malcolm H. Levitt[†]

*School of Chemistry, University of Southampton, Southampton, SO17 1BJ, United Kingdom*

Water exists in two forms, para and ortho, that have nuclear spin states with different symmetries. Here we report the conversion of fullerene-encapsulated para water to ortho water. The enrichment of para water at low temperatures is monitored via changes in the electrical polarizability of the material. Upon rapid dissolution of the material in toluene the excess para water converts to ortho water. In $H_2{}^{16}O@C_{60}$ the conversion leads to a slow increase in the NMR signal. In $H_2{}^{17}O@C_{60}$ the conversion gives rise to weak signal enhancements attributed to quantum-rotor-induced nuclear spin polarization. The time constants for the para-to-ortho conversion of fullerene-encapsulated water in ambient temperature solution are estimated as $30 \pm 4$ s for the $^{16}O$ isotopolog of water, and $16 \pm 3$ s for the $^{17}O$ isotopolog.

The wave function of a water molecule is antisymmetric under the exchange of its two protons, and may be written as a product of a rotational state and a nuclear spin state. Two different spin isomers of water exist: In para water the rotational state is symmetric, with an antisymmectric nuclear spin state with total spin $I = 0$. In ortho water the rotational state is antisymmetric, and the nuclear spin state is one of the three symmetric triplet states, with total spin $I = 1$. The rotational ground states of free para and ortho water have $J = 0$ and $J = 1$, respectively, and exhibit a splitting of 34 K [1].

The ratio of water spin isomers has been used to estimate the formation temperature of water in astrophysics [2,3]. Differences in the magnetic and electric properties have been used to separate the spin isomers in molecular beam experiments [4,5]. The conversion of water between its spin isomers has been followed at low temperatures by infrared spectroscopy [6,7] in inert gas matrices. A remarkable lifetime of 26 min has been claimed for bulk para water under ambient conditions [8], although this claim has been disputed [9,10].

The molecular endofullerene $H_2O@C_{60}$, produced by multistep chemical synthesis [11,12], provides an excellent system for studying water spin isomers. Each $C_{60}$ fullerene cage encapsulates a single water molecule which retains free molecular rotation at low temperatures [1,13]. The cage prevents the exchange of protons between water molecules, which provides a mechanism for rapid ortho-para equilibration in bulk water [14]. Spin-isomer conversion in water endofullerenes has been studied by infrared spectroscopy, neutron scattering, NMR, and via changes in dielectric constant [1,13,15,16]. The conversion of ortho water to para water follows second order kinetics, indicating that it is facilitated by water-water interactions

that may involve the electric dipole moments of neighboring water molecules [15].

Here we report on the conversion between para water and ortho water spin isomers in the endofullerene $H_2O@C_{60}$, in room-temperature solution. Alongside the spin-isomer conversion, we also observe weak nuclear spin polarization effects for water molecules bearing a $^{17}O$ nucleus. These quantum-rotor-induced polarization (QRIP) effects are related to analogous effects observed in unhindered $^{13}C$-bearing methyl ($CH_3$) rotors [17–19].

The $^1H$ NMR spectrum of $H_2O@C_{60}$, with a $^{17}O$ labeling level of 85% and dissolved in deuterated ortho-dichlorobenzene (ODCB), is shown in Fig. 1. The $^1H$ NMR spectrum exhibits six peaks due to the $J$ coupling of the two equivalent protons to the spin-$5/2$ $^{17}O$ nucleus. The linewidths of the $^1H$ NMR peaks are dominated by $^{17}O$ quadrupolar relaxation [20]. The sharp central peak is due to the 15% of molecules bearing the $^{16}O$ isotope. At 25 °C the $^1H$ $T_1$ values were reported previously to be $700 \pm 50$ ms for $H_2{}^{16}O@C_{60}$, and $750 \pm 50$ ms for $H_2{}^{17}O@C_{60}$. The $^{17}O$ $T_1$ is $81 \pm 7$ ms [20].

The ortho-$H_2O$ ground state in $H_2O@C_{60}$ is approximately 2.7 meV higher in energy than the para-$H_2O$ ground state, as determined by neutron scattering [1]. Hence temperatures below $\sim 20$ K strongly favor the para $H_2O$ state in thermal equilibrium. Figure 1(c) shows the equilibrium proportions of ortho $H_2O$ and para $H_2O$ as a function of temperature.

In the current work, we enhanced the fraction of para $H_2O$ by thermal equilibration at low temperature, and raised the temperature rapidly by dissolving the material in a warm solvent. The $^1H$ NMR spectrum was observed while para water converts back to ortho water at ambient temperature.
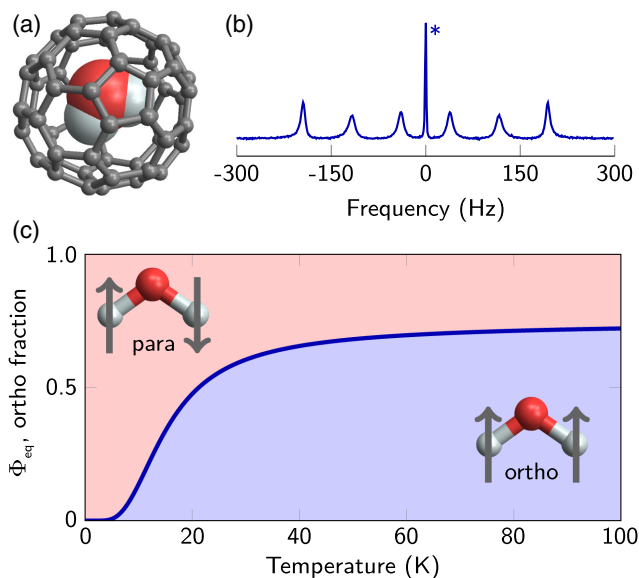
FIG. 1. (a) Molecular structure of $H_2O@C_{60}$. (b) $^1H$ NMR spectrum of $H_2O@C_{60}$, with a $^{17}O$ labeling level of 85%, dissolved in deuterated ortho dichlorobenzene. The proton resonance is split into a sextet due to the $J$ coupling to the spin-5/2 oxygen. The central line is due to the 15% of water bearing the $^{16}O$ isotope. (c) Equilibrium ortho fraction as a function of temperature. At high temperatures, 75% of the molecules are in the ortho state. At 5 K and in thermal equilibrium, the ortho state is almost completely depleted.

One experimental difficulty is that solid $H_2O@C_{60}$, just like $C_{60}$, dissolves only slowly, due to strong intermolecular interactions. Since slow dissolution is incompatible with observation of the rapid para-to-ortho conversion process, we first dissolved $H_2O@C_{60}$ in deuterated ODCB, at a concentration of 17 mM [21]. Dissolution proceeds rapidly when the frozen solid solution is exposed to warm solvent.

The kinetics of ortho-para conversion in pure $H_2O@C_{60}$ solid indicate that interactions between water molecules are important for the spin-isomer conversion process [15]. The use of a frozen solution generates uncertainty as to whether the water molecules in the frozen endofullerene solution do become enriched in the para spin isomer. The required predissolution of $H_2O@C_{60}$ in ODCB increases the distance between water molecules, and may change, and potentially suppress, the conversion to para water.

To resolve this issue we studied the ortho-para conversion of $H_2{}^{16}O@C_{60}$ in frozen ODCB solution by measuring the dielectric constant of the material. The electric polarizability of ortho water is larger than that of para water, in their respective rotational ground states. As water converts from ortho water to para water, the dielectric constant decreases. The techniques and analysis are similar to those reported in Ref. [16]. A new dielectric probe was constructed that can be loaded with liquid samples. The probe comprises three nearly identical, cylindrical capacitors that were loaded with solutions of $C_{60}$ in ODCB, $H_2{}^{16}O@C_{60}$ in ODCB, and
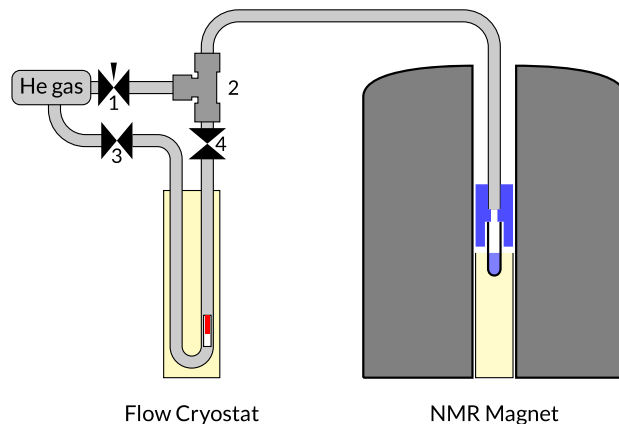


FIG. 2. Apparatus for rapid dissolution. Approximately 50 $\mu L$ of sample (red) are pipetted into a Teflon bullet which is then immersed in liquid nitrogen. For loading, the tube at the top of the union (2) is disconnected, the ball valve (4) is opened, and the bullet is pushed to the bottom of the steel tube. A small flow of helium gas, applied via the needle valve (1), prevents contamination of the system with air. The capsule is ejected by opening valves (3) and (4) and is propelled into the NMR magnet (right), where a 3D printed receiver (blue) retains the capsule and vents the helium gas. The sample travels further into the 5 mm NMR tube where it dissolves in warm solvent.

$H_2{}^{17}O@C_{60}$ in ODCB, respectively. The dielectric data show that spin conversion does occur, and leads to an estimated para fraction of 0.4 after 28 h at 4.2 K. Details of the dielectric probe, the measurement, and analysis are given in the Supplemental Material [22].

In order to observe spin-isomer conversion at ambient temperature, the sample is dissolved and the spectra are recorded using a liquid-state NMR apparatus. We rapidly dissolved the sample using a homebuilt pneumatic shuttle, shown in Fig. 2. A 1/4" steel tube (Swagelok, U.K.) was bent into a $U$ shape, the ends were fed through a KF-50 brass blank (Kurt Lesker, U.K.), and the tubing was brazed to the blank. Manual plug valves (Swagelok) are used to open and close the tube on either end. A small flow of helium gas is applied via a needle valve (Swagelok), to prevent contamination of the system with air during loading and ejection. The transfer of the sample to the secondary magnet takes approximately 100 ms. A 3D printed receiver structure retains the sample capsule and vents the helium gas, but allows the sample to travel further into a 5 mm NMR tube preloaded with warm solvent. A detailed drawing of the receiver structure is provided in the Supplemental Material [22]. The shuttle enables dissolution with a much smaller solvent volume than previous procedures [24], with gains in concentration and sensitivity that are critical for the experiments described here. The shuttle is mounted in a commercial flow cryostat (Oxford Instruments), that is located, for an unrelated purpose, in a 6.7 Tesla magnet. The field has no significant effect on the ortho-to-para conversion, but leads to a magnetization of the ortho water.
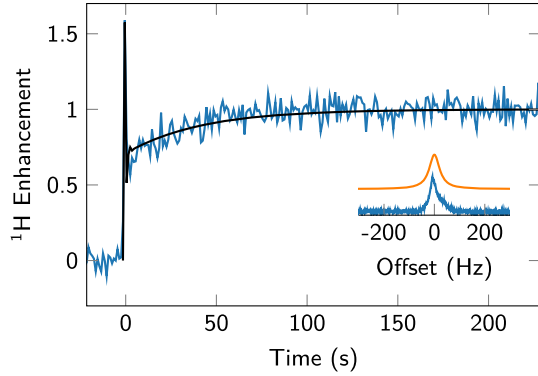
FIG. 3. Intensity of the $^1$H NMR signal of $H_2{}^{16}O@C_{60}$ in solution as a function of time (blue curve). Acquisition starts prior to arrival of the sample. The time origin is chosen to coincide with the first NMR signal after dissolution of the sample. The initial sharp peak is due to initial ortho-water magnetization (the cryostat is located in a 6.7 Tesla magnet), and decays rapidly with the proton $T_1$. Following the rapid decay the signal intensity increases with time as para water converts to ortho water. The black curve shows the result of a spin dynamical simulation with a time constant $T_S = 30$ s for the conversion of para water to ortho water (see text). The inset shows a spectrum (lower, blue curve) obtained from averaging 20 transients recorded 8 min after dissolution of the sample, and a Lorentzian mask (upper, orange curve) that was applied prior to integration.

Separate experiments were conducted to study the para-ortho conversion of $H_2{}^{16}O@C_{60}$ and $H_2{}^{17}O@C_{60}$. In the first experiment a sample of 50 $\mu$L $H_2{}^{16}O@C_{60}$ in ODCB was kept at a temperature of 3.9 K for approximately 15 h. $^1$H NMR spectra were recorded every 1 s using a flip angle of approximately 30°. Acquisition of NMR data was started approximately 20 s before the sample was ejected from the cryostat and dissolved in the NMR tube. The obtained spectra were multiplied with a Lorentzian mask and integrated to obtain the NMR signal intensity, shown in Fig. 3.

The sharp peak in the NMR signal immediately after dissolution is attributed to the nuclear magnetization of ortho water which was prepolarized by keeping the sample in a magnetic field at low temperatures. This peak decays rapidly with the proton $T_1$ of ~0.8 s. Subsequently, the signal intensity slowly increases as para water converts to ortho water.

Results of an analogous experiment, conducted on $H_2{}^{17}O@C_{60}$, are shown in Fig. 4. For this experiment, the sample was kept at a temperature of 4 K for approximately 15 h. $^1$H NMR spectra were recorded every 250 ms using a flip angle of approximately 30°.

Figure 4(b) shows the evolution of the NMR spectrum after dissolution of the sample. Spectra were averaged over a total acquisition time of 5 s to improve the signal-to-noise ratio. Spectra averaged during the first 5 s clearly show an antiphase pattern that is characteristic for QRIP [19,25,26]. The time evolution of the individual peaks is obtained by multiplying the spectra with Lorentzian masks as shown in

panel (c), followed by integration. The corresponding trajectories for the six $H_2{}^{17}O@C_{60}$ peaks, normalized by their respective thermal intensities and with a tricube bandwidth reduction of width 2 s, are shown in panel (d). The procedure is detailed in the Supplemental Material [22] which includes Ref. [27]. Panels (e)–(j) show separate plots of the six peak intensities, together with trajectories obtained from spin dynamical simulations. The outermost peaks exhibit small enhancements of up to 2. A thermal equilibrium spectrum is shown in Fig. 4(a).

Simulations of the proton peak trajectories during the spin-isomer conversion process of both $H_2{}^{16}O@C_{60}$ and $H_2{}^{17}O@C_{60}$ were performed by using SPINDYNAMICA software with a modified thermalization procedure (see below) [28–32]. The simulations for $H_2{}^{16}O$ included $^1$H-$^1$H dipole relaxation and spin rotation. In the case of $H_2{}^{17}O$, $^1$H-$^{17}$O dipole-dipole relaxation, $^{17}$O quadrupolar relaxation, and their cross-correlations were also included, along with the experimentally observed $^1$H-$^{17}$O $J$ coupling of 77.9 Hz.

The relevant interactions were derived from the known molecular geometry and the $^{17}$O quadrupole coupling constant of 10.11 MHz [33]. In order to match the experimentally observed relaxation time of 86 ms for the $^{17}$O longitudinal magnetization, a rotational correlation time of $\tau_C = 107$ fs was used for the simulation of both water isomers [20].

An external random field contribution, characterized by the magnitude of the random fields and correlation coefficients $\kappa_{i,j}$ [25], was included in order to model spin-rotation coupling. All relaxation processes were treated by using a relaxation superoperator in the isotropic fast-motion limit as detailed in Ref. [20]. A random field of $\eta_H^{rand2}\tau^{rand} = 0.6$ s$^{-1}$ was used to model spin-rotation relaxation in order to match the experimentally observed longitudinal relaxation time of 755 ms for the proton spins.

The time constant for the para-to-ortho equilibration is related to the rates for para-to-ortho conversion, $k_{p\rightarrow o}$ and the reverse process, $k_{o\rightarrow p}$, as follows:

$$T_S^{-1} = 4k_{p\rightarrow o} = \frac{4}{3}k_{o\rightarrow p}. \tag{1}$$

The time constant for para-to-ortho conversion is denoted here $T_S$, since this quantity corresponds precisely to the decay time constant of singlet order, in the NMR of long-lived spin states [29–31]. The relaxation superoperator yields the following expressions for $k_{p\rightarrow o}$ for the two water isotopologs:

$$k_{p\rightarrow o}(H_2{}^{16}O) = \eta_H^{rand2}\tau^{rand}(1 - \kappa), \tag{2}$$

$$k_{p\rightarrow o}(H_2{}^{17}O) = k_{p\rightarrow o}(H_2{}^{16}O) + k_{DD}^{OH}. \tag{3}$$

For $^{16}$O, good agreement with experimental data is found for $T_S(H_2{}^{16}O) = 30 \pm 4$ s, corresponding to $\kappa = 0.986 \pm 0.002$ (black curve in Fig. 3).

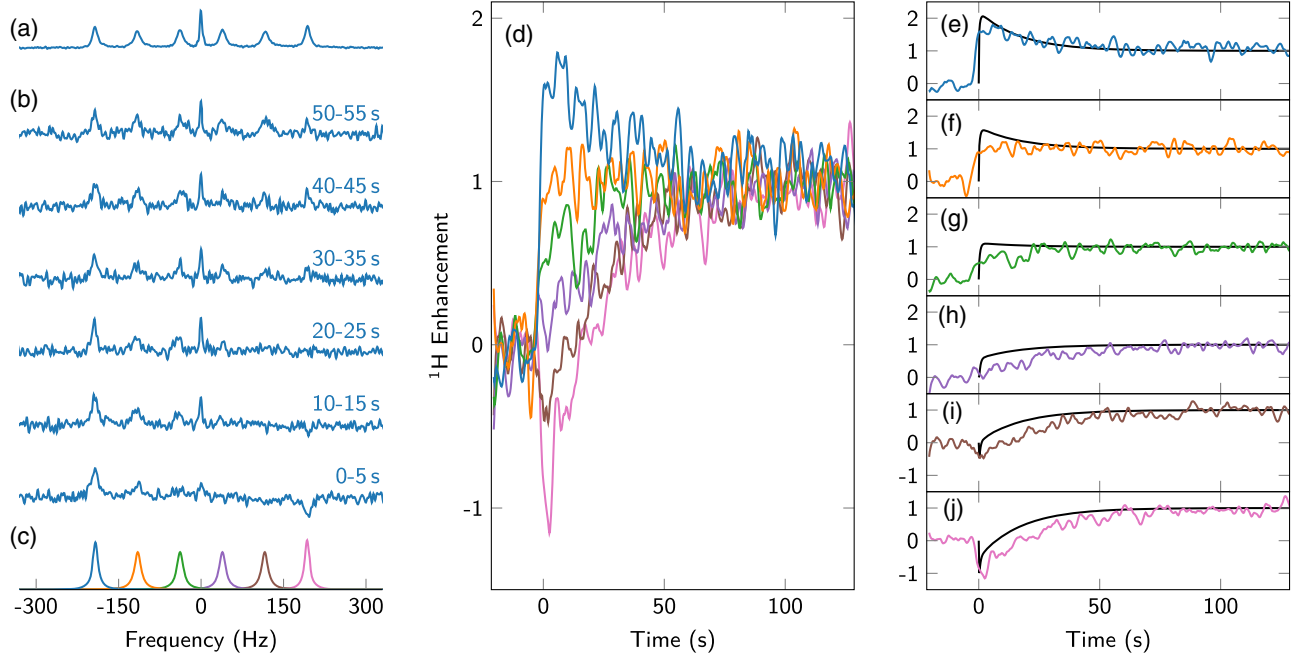FIG. 4.   QRIP Experiment on $H_2{}^{17}O@C_{60}$. (a) Thermal equilibrium $^1H$ spectrum, recorded after equilibration of the sample (1024 transients averaged). (b) Averages of 20 transients during consecutive intervals after dissolution of the sample. A clear antiphase signal is obtained immediately after the dissolution (0–5 s). The antiphase signal decays, and after approximately one minute the thermal signal is restored. (c) The individual spectra are multiplied with Lorentzian masks that correspond to each of the six peaks, and the product is integrated. (d) Results of the integration after applying a tricube bandwidth reduction of width 2 s. The integrals are normalized by the intensity of the respective thermal $^{17}O$ peaks. (e)–(j) The same data as in (d), with spin dynamical simulations (black lines).

In the case of $H_2{}^{17}O$, $k_{DD}^{OH}$ accounts for the additional contribution of the $^1H$-$^{17}O$ dipole-dipole interactions. A general expression has been given in Eq. (4) of Ref. [34]. Here the couplings of the protons to the spin 5/2 hetero-nucleus are identical, and the expression simplifies to

$$k_{DD}^{OH} = \frac{35}{4} \left( \frac{\hbar \mu_0 \gamma^{17O} \gamma^{1H}}{4\pi \, r^3} \right)^2 \tau_C \sin^2\theta = 0.0087 \text{ s}^{-1}, \quad (4)$$

where $\gamma^{17O}$ and $\gamma^{1H}$ are the gyromagnetic ratios of $^{17}O$ and $^1H$, respectively, and $\tau_C$ is the correlation time, assumed to be $\tau_C = 107$ fs. The numeric result is obtained using the $^1H$-$^{17}O$-distance $r$ and the H-O-H angle $\theta$ of the endohedral molecule from quantum chemistry calculations [35]. For $H_2{}^{17}O@C_{60}$ good agreement with experimental data is found for $\kappa \in [0.99, 1]$, corresponding to $T_S(H_2{}^{17}O) = 16 \pm 3$ s.

This analysis shows that the experimental data and theory may only be reconciled by assuming a very high degree of correlation for the random fields used to model the spin-rotation interaction. Numerical simulations indicate that contributions from quadrupolar relaxation have negligible influence on the para-to-ortho conversion kinetics.

In NMR, the evolution of the spin density operator is typically described by the following master equation [36]:

$$\dot{\rho}(t) = -i\hat{H}_{coh}\rho(t) + \hat{\Gamma}(\rho(t) - \rho_{eq}), \quad (5)$$

where $\hat{H}_{coh}$ is the commutation superoperator of the coherent Hamiltonian and $\rho_{eq}$ the thermal equilibrium density operator. This equation is a good approximation for spin systems which are close to thermal equilibrium, but leads to incorrect results for spin systems that are far from equilibrium, which is the case here. The simulations shown in Figs. 3 and 4 made use of the homogeneous master equation [37,38]:

$$\dot{\rho}(t) = -i\hat{H}_{coh}\rho(t) + \hat{\Gamma}_\theta(\rho(t)). \quad (6)$$

The thermally corrected relaxation superoperator $\hat{\Gamma}_\theta$ is given by

$$\hat{\Gamma}_\theta = \hat{\Gamma} \exp\left( \hat{H}_{lab}^L \hat{P}_D / (k_B T) \right), \quad (7)$$

where $\hat{H}_{lab}^L$ is the left translation superoperator [36] of the laboratory-frame coherent Hamiltonian $H_{lab}$ and $\hat{P}_D$ is the diagonal part projector with respect to the Hamiltonian $H_{lab}$ [39]. Unlike the forms proposed in Refs. [37,38], this superoperator respects detailed balance [39] and provides physically reasonable results even for spin systems far from thermal equilibrium.

The density operator immediately after dissolution is determined by the initial fraction of para water and ortho water. The initial fractions are not known a priori and were adjusted to give the best agreement between simulations and data. The simulation results are shown as black curves

in Figs. 3 and 4(e)–4(j) for $H_2{}^{16}O@C_{60}$ and $H_2{}^{17}O@C_{60}$, respectively. The initial para fractions are estimated as $54 \pm 15\%$ and $43 \pm 3\%$, respectively, where the larger uncertainty for $H_2{}^{16}O@C_{60}$ is due to the smaller dynamic range of the $H_2{}^{16}O$ data.

In conclusion, NMR experiments were used to study the spin-isomer conversion for the endohedral water molecules of $H_2O@C_{60}$ in ambient-temperature solution. The time constants for the para and ortho equilibration are found to be $30 \pm 4$ s for the $^{16}O$ isotopolog of water, and $16 \pm 3$ s for the $^{17}O$ isotopolog. The faster para-to-ortho conversion of $H_2{}^{17}O$ is attributed to $^{1}H$-$^{17}O$ dipole-dipole interactions. Weak nuclear spin polarization effects are observed for the $^{17}O$ isotopolog as the spin-isomer conversion proceeds. Measurements of electrical capacitance at low temperature indicate that slow conversion between the water spin isomers also takes place in frozen solutions of $H_2O@C_{60}$ in ODCB, with the conversion again proceeding more rapidly for the $^{17}O$ isotopolog than for the $^{16}O$ species.

---

*b.meier@soton.ac.uk
†mhl@soton.ac.uk

[1] C. Beduz, M. Carravetta, J. Y.-C. Chen, M. Concistrè, M. Denning, M. Frunzi, A. J. Horsewill, O. G. Johannessen, R. Lawler, X. Lei *et al.*, Proc. Natl. Acad. Sci. U.S.A. **109**, 12894 (2012).
[2] T. Encrenaz, Annu. Rev. Astron. Astrophys. **46**, 57 (2008).
[3] M. R. Hogerheijde, E. A. Bergin, C. Brinch, L. I. Cleeves, J. K. J. Fogel, G. A. Blake, C. Dominik, D. C. Lis, G. Melnick, D. Neufeld, O. Panic, J. C. Pearson, L. Kristensen, U. A. Yildiz, and E. F. van Dishoeck, Science **334**, 338 (2011).
[4] T. Kravchuk, M. Reznikov, P. Tichonov, N. Avidor, Y. Meir, A. Bekkerman, and G. Alexandrowicz, Science **331**, 319 (2011).
[5] D. A. Horke, Y.-P. Chang, K. Długołęcki, and J. Küpper, Angew. Chem., Int. Ed. **53**, 11965 (2014).
[6] R. L. Redington and D. E. Milligan, J. Chem. Phys. **39**, 1276 (1963).
[7] P.-A. Turgeon, P. Ayotte, E. Lisitsin, Y. Meir, T. Kravchuk, and G. Alexandrowicz, Phys. Rev. A **86**, 062710 (2012).
[8] V. I. Tikhonov, Science **296**, 2363 (2002).
[9] P. Cacciani, J. Cosléou, and M. Khelkhal, Phys. Rev. A **85**, 012521 (2012).
[10] S. L. Veber, E. G. Bagryanskaya, and P. L. Chapovsky, J. Exp. Theor. Phys. **102**, 76 (2006).
[11] K. Kurotobi and Y. Murata, Science **333**, 613 (2011).
[12] A. Krachmalnicoff, M. H. Levitt, and R. J. Whitby, Chem. Commun. **50**, 13037 (2014).
[13] K. S. K. Goh, M. Jiménez-Ruiz, M. R. Johnson, S. Rols, J. Ollivier, M. S. Denning, S. Mamone, M. H. Levitt, X. Lei, Y. Li, N. J. Turro, Y. Murata, and A. J. Horsewill, Phys. Chem. Chem. Phys. **16**, 21330 (2014).
[14] D. Mammoli, N. Salvi, J. Milani, R. Buratto, A. Bornet, A. A. Sehgal, E. Canet, P. Pelupessy, D. Carnevale, S. Jannin, and G. Bodenhausen, Phys. Chem. Chem. Phys. **17**, 26819 (2015).
[15] S. Mamone, M. Concistrè, E. Carignani, B. Meier, A. Krachmalnicoff, O. G. Johannessen, X. Lei, Y. Li, M. Denning, M. Carravetta, K. Goh, A. J. Horsewill, R. J. Whitby, and M. H. Levitt, J. Chem. Phys. **140**, 194306 (2014).
[16] B. Meier, S. Mamone, M. Concistrè, J. Alonso-Valdesueiro, A. Krachmalnicoff, R. J. Whitby, and M. H. Levitt, Nat. Commun. **6**, 8112 (2015).
[17] M. Icker and S. Berger, J. Magn. Reson. **219**, 1 (2012).
[18] M. Icker, P. Fricke, T. Grell, J. Hollenbach, H. Auer, and S. Berger, Magn. Reson. Chem. **51**, 815 (2013).
[19] B. Meier, J.-N. Dumez, G. Stevanato, J. T. Hill-Cousins, S. S. Roy, P. Håkansson, S. Mamone, R. C. D. Brown, G. Pileio, and M. H. Levitt, J. Am. Chem. Soc. **135**, 18746 (2013).
[20] S. J. Elliott, C. Bengs, K. Kouril, B. Meier, S. Alom, R. J. Whitby, and M. H. Levitt, ChemPhysChem **19**, 251 (2018).
[21] N. O. Mchedlov-Petrossyan, Chem. Rev. **113**, 5149 (2013).
[22] See Supplemental Material at http://link.aps.org/supplemental/10.1103/PhysRevLett.120.266001 for technical details of the dielectric probe and the receiver for rapid dissolution experiments, as well as for capacitance data, data processing and modeling [23], and data on the ortho-para conversion in solid fullerene samples.
[23] Y.-P. Chang, F. Filsinger, B. G. Sartakov, and J. Küpper, Comput. Phys. Commun. **185**, 339 (2014).
[24] J. H. Ardenkjær-Larsen, B. Fridlund, A. Gram, G. Hansson, L. Hansson, M. H. Lerche, R. Servin, M. Thaning, and K. Golman, Proc. Natl. Acad. Sci. U.S.A. **100**, 10158 (2003).
[25] J.-N. Dumez, P. Håkansson, S. Mamone, B. Meier, G. Stevanato, J. T. Hill-Cousins, S. S. Roy, R. C. D. Brown, G. Pileio, and M. H. Levitt, J. Chem. Phys. **142**, 044506 (2015).
[26] S. S. Roy, J.-N. Dumez, G. Stevanato, B. Meier, J. T. Hill-Cousins, R. C. Brown, G. Pileio, and M. H. Levitt, J. Magn. Reson. **250**, 25 (2015).
[27] P. K. Janert, *Data Analysis with Open Source Tools* (O'Reilly, Sebastopol, 2010).
[28] C. Bengs and M. H. Levitt, Magn. Reson. Chem. **56**, 374 (2017).
[29] M. Carravetta, O. G. Johannessen, and M. H. Levitt, Phys. Rev. Lett. **92**, 153003 (2004).
[30] G. Pileio, Prog. Nucl. Magn. Reson. Spectrosc. **56**, 217 (2010).
[31] M. H. Levitt, Annu. Rev. Phys. Chem. **63**, 89 (2012).
[32] G. Stevanato, J. T. Hill-Cousins, P. Håkansson, S. S. Roy, L. J. Brown, R. C. D. Brown, G. Pileio, and M. H. Levitt, Angew. Chem., Int. Ed. **54**, 3740 (2015).

[33] L. Olsen, O. Christiansen, L. Hemmingsen, S. P. A. Sauer, and K. V. Mikkelsen, J. Chem. Phys. **116**, 1424 (2002).

[34] G. Pileio, J. T. Hill-Cousins, S. Mitchell, I. Kuprov, L. J. Brown, R. C. D. Brown, and M. H. Levitt, J. Am. Chem. Soc. **134**, 17494 (2012).

[35] A. B. Farimani, Y. Wu, and N. R. Aluru, Phys. Chem. Chem. Phys. **15**, 17993 (2013).

[36] R. R. Ernst, G. Bodenhausen, and A. Wokaun, *Principles of Nuclear Magnetic Resonance in One and Two Dimensions* (Oxford University Press, Oxford, 1987).

[37] J. Jeener, Adv. Magn. Reson. **10**, 1 (1982).

[38] M. H. Levitt and L. Di Bari, Phys. Rev. Lett. **69**, 3124 (1992).

[39] T. Levante and R. Ernst, Chem. Phys. Lett. **241**, 73 (1995).